Challenge Journal of Structural Mechanics

Research Article

A discrete element method for evaluating the seismic performance of concrete gravity dam-reservoir systems under main shock-aftershock events

Berat Feyza Soysal [a,*]

[a] *Department of Civil Engineering, Çankaya University, 06815 Ankara, Türkiye*

ABSTRACT

Dams are crucial for water supply, flood prevention, and hydroelectric power generation. Often located in seismically active regions, they are vulnerable to main shock-aftershock (MS-AS) sequences, which can compromise structural integrity and hydraulic safety. Critical aspects of dam response to MS–AS events remain unclear, particularly the required rest time between successive events and threshold AS-to-MS intensity measure ratios that could serve as predictors of additional damage. This study addresses these gaps by analyzing concrete gravity dam–reservoir systems of three heights (50 m, 100 m, and 150 m) using the developed discrete element–based approach coupled with displacement/pressure-based mixed finite elements for the reservoir. Empirical rest time equations were derived from 124 as-recorded ground motions, while seismic performance under varying intensity levels was evaluated using 14 as-recorded MS–AS sequences. Damage was quantified using discrete indices of base crack length, maximum base crack width, and maximum total upstream crack width. Results indicate that AS primarily propagate existing cracks at lower intensities, whereas higher intensities generate new cracks along the upstream face, increasing crack widths by 25–30% on average. The 50 m high dam remained within the mild damage category, while taller dams occasionally reached moderate levels, posing potential seepage risks. Threshold AS-to-MS ratios for four different intensity measures were identified. These findings provide mechanistic insight into crack propagation under MS-AS events, providing practical guidance for post-earthquake dam safety assessment, inspection prioritization, and incorporating sequential seismic effects into design and emergency planning.

ARTICLE INFO

Article history:
Received – July 2, 2025
Revision requested – August 19, 2025
Revision received – September 12, 2025
Accepted – September 24, 2025

Keywords:
Concrete gravity dam-reservoir system
Crack width
Discrete element modeling
Main shock-aftershock sequence
Seismic intensity measure

Citation: Soysal BF (2025). A discrete element method for evaluating the seismic performance of concrete gravity dam-reservoir systems under main shock-aftershock events. *Challenge Journal of Structural Mechanics*, 11(4), 229–244.

1. Introduction

Dams are crucial structures constructed for water storage. The stored water in the reservoir is used to supply water, prevent floods, and generate hydroelectric power. The Jawa Dam, located in Jordan and constructed around 3000 BC, is recognized as the earliest known dam (Fahlbusch 2009). As of 2023, the global count of dams exceeds 62000 (ICOLD 2023). Given their frequent construction in active seismic zones (SRC n.d.), dams necessitate seismic performance evaluations (Hacıefendioğlu et al. 2015; Akköse et al. 2016) due to the potential for catastrophic loss of life and severe property damage upon failure.

Earthquakes consist of foreshocks, main shocks, and aftershocks. While foreshocks can indicate an impending earthquake, their typically smaller magnitudes (Mignan 2014) preclude significant structural damage.

* *Corresponding author*. Tel.: +90-312-233-1402 ; E-mail address: fsoysal@cankaya.edu.tr (B. F. Soysal)
ISSN: 2149-8024 / DOI: https://doi.org/10.20528/cjsmec.2025.04.005

However, historical earthquake events have demonstrated that aftershocks can exhibit magnitudes comparable to main shocks (Risk Management Solutions 2008; Wen et al. 2009; USGS 2015). If a structure is already damaged by a main shock, a subsequent strong aftershock can intensify the structural damage, potentially leading to collapse (Alliard and Leger 2008; Hariri-Ardebili and Kianoush 2014; Pang et al. 2019; Sadeghi and Moradloo 2022). Many studies have confirmed this effect. Analyses of single-degree-of-freedom (SDOF) systems revealed increased damage accumulation under seismic sequences (Amadio et al. 2003; Hatzigeorgiou and Beskos 2009; Hatzigeorgiou 2010). Investigations of steel frames (Amadio et al. 2003; Fragiacomo et al. 2004) and concrete frames (Faisal et al. 2013) demonstrated that aftershocks substantially increased damage. Similarly, Guo et al. (2020) proposed a fragility function including aftershocks and showed that strong aftershocks increased bridge collapse probabilities.

Concrete dams are also vulnerable to main shock-aftershock (MS–AS) sequences. Alliard and Leger (2008) analyzed a gravity dam considering reduced drainage efficiency after main shocks and found that aftershocks could induce additional damage and sliding displacements. The seismic performance of the Koyna Gravity Dam under MS–AS sequences has been investigated extensively (Zhang et al. 2013; Wang et al. 2017, 2020; Sadeghi and Moradloo 2022; Ashna et al. 2024). Reported damage measures included local and global damage indices (Zhang et al. 2013; Wang et al. 2017; Ashna et al. 2024), crest displacement (Wang et al. 2017, 2020), damage patterns (Wang et al. 2020), and sliding of the top block (Sadeghi and Moradloo 2022). These studies consistently showed that the dam's neck region was particularly susceptible to aftershocks, with strong aftershocks leading to greater damage accumulation. Similar findings were reported for other gravity dam–foundation systems (Zhang et al. 2019, 2021; Zhai et al. 2022) and for arch (Hariri-Ardebili and Kianoush 2014) and CFRD dams (Pang et al. 2019). More recently, Akpinar et al. (2023) investigated post-seismic effects without explicitly applying aftershocks and found increased damage in concrete gravity dams.

A crucial aspect of successive seismic analyses is determining the appropriate time interval between the main shock and aftershocks, ensuring the structure returns to a resting state before the subsequent seismic event. For SDOF and steel frames, Pirooz et al. (2021) proposed formulations to estimate this interval. However, no comprehensive rest time study exists for dams. Previous research employed intervals ranging from 10 seconds (Pang et al. 2019; Wang et al. 2017, 2020; Zhang et al. 2019, 2021; Zhai et al. 2022; Ashna et al. 2024) to 100 seconds (Zhang et al. 2013).

Although prior studies have confirmed the damaging potential of aftershocks, several key issues remain unresolved. No empirical data are available on the required rest time between consecutive seismic events for dam–reservoir systems. Threshold values of aftershock-to-main shock intensity measure ratios that can serve as predictors of damaging aftershocks have not been established. Moreover, most existing analyses considered only a single dam height and a limited number of MS–AS sequences, while relying mainly on finite element methods that cannot directly compute discrete damage indices such as crack widths.

This study introduces a discrete element–based framework developed by the author to directly model crack initiation and propagation in dam–reservoir systems of varying heights. The novelty lies in (i) developing empirical rest time equations for dam–reservoir systems of different heights, and (ii) identifying threshold aftershock-to-main shock intensity measure ratios that can serve as predictors of damaging aftershocks. These contributions provide practical indicators directly linked to discrete damage indices such as base crack length, maximum base crack width, and maximum total crack width on the upstream face, the latter being particularly relevant for seepage risks.

The manuscript is organized as follows: Section 2 presents the theoretical formulation of the MAEM and the displacement/pressure-based mixed finite element reservoir model. Section 3 provides validation of these models using three different benchmark cases. Section 4 describes the dam–reservoir models and input ground motions. Section 5 presents the proposed rest time equations. Section 6 evaluates the seismic performance of dam systems by means of discrete damage indices for various seismicity levels and examines the influence of ground motion parameters, and Section 7 summarizes the conclusions.

2. Theory and Formulation

2.1. Modified applied element method

The Applied Element Method (AEM) is a discrete element-based approach where a structure is discretized into rigid elements interconnected by normal and shear spring pairs (Meguro and Tagel-Din 2000). This method is modified (MAEM) by incorporating two additional diagonal springs between elements to accurately model Poisson's effect (Fig. 1(a)). The stiffness values for the normal (k_n), shear (k_s), and diagonal, (k_{nd}) springs, which represent the macroscopic material properties of Young's modulus (E) and Poisson's ratio (ν), are calculated based on the Cauchy-Born rule and hyper-elastic theory (Eq. 1). The details of the formulation of MAEM can be found in Soysal et al. (2023).

$$k_n = \frac{Et}{(1+\nu)s} \quad k_n = \frac{Et}{(1+\nu)s} \quad k_{nd} = \frac{Et\nu}{(1-\nu^2)} \tag{1}$$

In Eq. (1), t denotes the thickness of the structure, and s represents the number of normal-shear spring pairs connecting the elements.

The nonlinear behavior of concrete, specifically tensile cracking, is modeled by implementing the Maekawa tension softening material model (Maekawa et al. 2003) (Fig. 1(b) and Eq. (2)). Mesh independence is achieved by incorporating fracture energy into the system (Soysal et al. 2023).

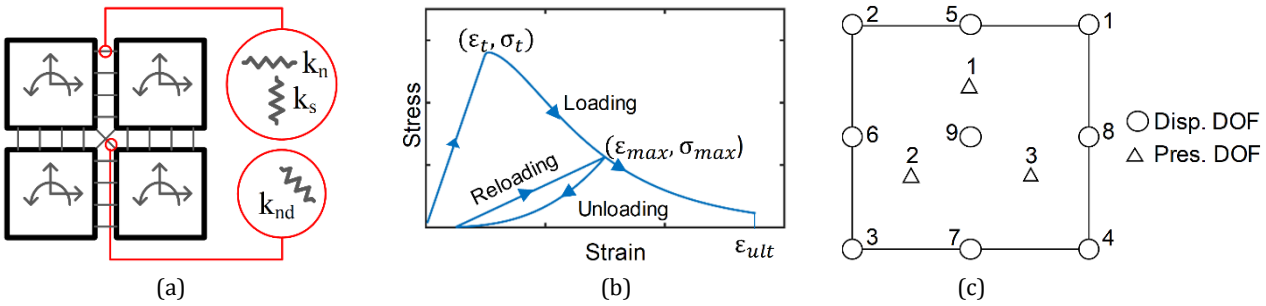

(a) (b) (c)

Fig. 1. Modified Applied Element Method and the reservoir element: (a) Modified applied elements; (b) Tension softening model; (c) Displacement/pressure-based mixed finite element.

Loading: $\varepsilon > \varepsilon_{\max}$

$$\sigma = \begin{cases} \frac{\sigma_t}{\varepsilon_t}\varepsilon & \text{if } \varepsilon \le \varepsilon_t \\ \sigma_t \left(\frac{\varepsilon_t}{\varepsilon}\right)^c & \text{if } \varepsilon_t < \varepsilon < \varepsilon_{\text{ult}} \\ 0 & \text{if } \varepsilon \ge \varepsilon_{\text{ult}} \end{cases}$$

Unloading: $\varepsilon \le \varepsilon_{\max}$ and $\varepsilon \le \varepsilon_0$

$$\sigma = E_{\text{ul}} \cdot \varepsilon \cdot \alpha$$

$$E_{ul} = \frac{\sigma_{\max}}{\varepsilon_{\max}} \text{ and } \alpha = \left(\frac{\sigma_0}{E_{\text{ul}}\varepsilon}\right)\left(\frac{\varepsilon}{\varepsilon_0}\right)^3$$

Reloading: $\varepsilon \le \varepsilon_{\max}$ and $\varepsilon > \varepsilon_0$

$$\sigma = \sigma_{\max} - (\sigma_{\max} - \sigma_0)\left(\frac{\varepsilon_{\max} - \varepsilon}{\varepsilon_{\max} - \varepsilon_0}\right) \quad (2)$$

Here, ε represents the tensile strain of concrete, σ is the corresponding tensile stress, σ_t is the uniaxial concrete tensile strength, and ε_t is the corresponding tensile cracking strain. c is the softening parameter that defines the post-peak behavior. $\varepsilon_{\max}$ and $\sigma_{\max}$ denote the maximum tensile strain experienced and its corresponding tensile stress, respectively. The current strain and stress are denoted as ε_0 and σ_0, respectively. The unloading stiffness is computed as $E_{\text{ul}}\alpha$, where α is the stiffness parameter.

For all springs, compressive behavior is assumed to be linear. Conversely, the shear springs exhibit brittle behavior. Once the normal spring pair enters the nonlinear loading regime (i.e., $\varepsilon \ge \varepsilon_t$), the corresponding shear spring pair loses its capacity to carry force or contribute to the system's stiffness.

2.2. Displacement/pressure-based mixed finite element

In this study, the dam-reservoir interaction is accounted for by coupling the modified applied elements with the displacement/pressure-based mixed finite elements proposed by Wang and Bathe (1997). The implemented finite element possesses nine displacement and three pressure degrees of freedom (Fig. 1(c)). The matrix formulation of the finite element is presented in Eq. (3).

$$\begin{bmatrix} \mathbf{M} & \mathbf{0} \\ \mathbf{0} & \mathbf{0} \end{bmatrix} \begin{bmatrix} \ddot{\widehat{\boldsymbol{U}}} \\ \ddot{\widehat{\boldsymbol{P}}} \end{bmatrix} + \begin{bmatrix} \mathbf{K}_{uu} & \mathbf{K}_{up} \\ \mathbf{K}_{pu} & \mathbf{K}_{pp} \end{bmatrix} \begin{bmatrix} \widehat{\boldsymbol{U}} \\ \widehat{\boldsymbol{P}} \end{bmatrix} = \begin{bmatrix} \boldsymbol{R} \\ \mathbf{0} \end{bmatrix} \quad (3)$$

In this equation, $\mathbf{M}$ denotes the mass term of the element, $\widehat{\boldsymbol{U}}$ and $\widehat{\boldsymbol{P}}$ are the displacement and pressure solution vectors, respectively, and $\mathbf{K}_{uu}$, $\mathbf{K}_{up}$, $\mathbf{K}_{pu}$, and $\mathbf{K}_{pp}$ represent the corresponding stiffness sub-matrices. The pressure unknowns can be statically condensed for a finite bulk modulus, simplifying the solution to Eq. (4).

$$\mathbf{M}\ddot{\widehat{\boldsymbol{U}}} + \left(-\mathbf{K}_{up}\,\mathbf{K}_{pp}^{-1}\,\mathbf{K}_{pu}\right)\widehat{\boldsymbol{U}} = \boldsymbol{R} \quad (4)$$

For almost incompressible materials, the displacement/pressure-based mixed formulation satisfies the inf-sup conditions, thereby eliminating spurious zero-energy modes (Wang and Bathe 1997).

The Sommerfeld radiation boundary condition (Sommerfeld 1949) is applied at the far end of the reservoir to account for radiating waves.

3. Validation Studies

Several validation studies, including pure tension, splitting tension, push-over loading of a scaled concrete dam, tensile testing of double-edged notched specimens, and the cracking response of the Koyna Dam-reservoir system, have been conducted to verify the MAEM and its coupling with fluid finite elements (Soysal Albostan 2021; Soysal et al. 2023). Further validation (Soysal and Arici 2024) was carried out by simulating the variability in concrete properties utilizing the random field theory (Wei et al. 2024). The direct tension test (Gopalaratnam and Shah 1985) and the push-over loading of a scaled concrete dam (Carpinteri et al. 1992) were modeled with five random samples, and the corresponding load-displacement and cracking behaviors were obtained. For brevity, this manuscript presents the cracking response of the Koyna Dam-reservoir system under nonlinear dynamic analysis, along with the aforementioned random field results. Detailed information on these validations can be found in the works of Soysal Albostan (2021), Soysal et al. (2023), and Soysal and Arici (2024).

The simulated damage in the Koyna Dam-reservoir system is compared with the observed damage in Fig. 2(a). The model successfully reproduced the localized cracking at the heel and neck of the dam. Additional cracks appeared on the downstream face, likely due to mesh discretization and localized stress concentrations. Overall, the simulated cracking pattern is compatible with the actual damage observed in the Koyna Dam.

The random field results for the direct tension test exhibited a similar distribution of load-displacement values around the experimental result. The crack patterns obtained were also consistent with the experimental findings (Fig. 2(b)). The robustness of the methodology was further demonstrated in the push-over test, where the load-CMOD response closely matched the experimental data. The resulting fracture patterns followed essentially the same crack path and agreed well with the experimental result (Fig. 2(c)).

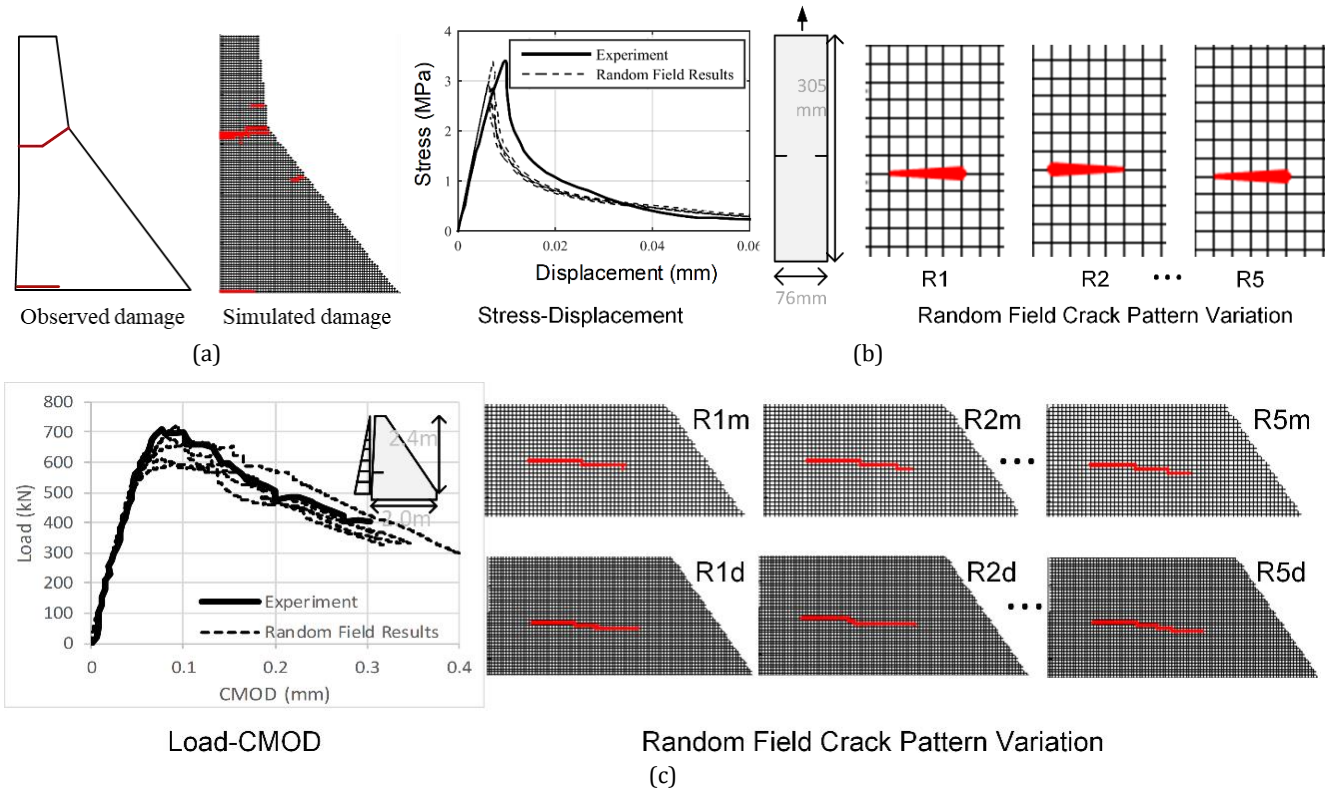

Fig. 2. Verification results: (a) Damage of Koyna Dam-reservoir system; (b) Random field results for direct tension test (Gopalaratnam and Shah 1985); (c) Random field results for push-over test (Carpinteri et al. 1992).

4. Dam Systems and Ground Motions

4.1. Coupled MAEM – Finite element models

The seismic performance of concrete gravity dam-reservoir systems under main shock-aftershock events was evaluated by considering three distinct concrete gravity dam sections: 50 m (Model I), 100 m (Model II), and 150 m in height (Model III) (Fig. 3). The cross-sectional properties of the dams were selected based on the "standard" dam cross-section (Chopra 1978; Lokke and Chopra 2013), featuring a vertical upstream face and a 0.8/1 downstream slope. The reservoir height was assumed to be 2 m lower than the dam height, and its length was three times the dam height. The dam body was discretized into 1m x 1m modified applied elements, while the reservoir mesh consisted of 2m x 8m finite elements. The Young's modulus, Poisson's ratio, tensile strength, and fracture energy of the concrete dams were assumed to be 28 GPa, 0.2, 2.4 MPa, and 200 N/m, respectively. The acoustic wave speed, Poisson's ratio, and water density for the reservoir were 1438.66 m/s, 0.4999, and 1000 kg/m^3, respectively. These material properties are within the typical range for concrete gravity dam-reservoir systems reported in the literature (Leger and Leclerc 1996; Hariri-Ardebili and Saouma 2016; Chen et al. 2019; Ghallab 2020), ensuring realistic material representation for a generic dam model where specific site data are unavailable. The first three frequencies of the systems are presented in Table 1. A 5% Rayleigh damping ratio, applied at the first and third modes of the systems, was utilized in the nonlinear transient analyses.

4.2. Selected earthquake ground motions

The required time interval between main shocks and aftershocks was estimated using 124 acceleration records from 21 different events, sourced from the PEER NGA-West2 (http://ngawest2.berkeley.edu) ground motion database and COSMOS strong motion virtual data center (https://www.strongmotioncenter.org/) (Table A1). These records had fault distances (R) of 0-85 km, magnitudes (M) of 5.3-7.6, and shear wave velocity ($V_{s,30}$) above 203 m/s, with the minimum value corresponding to stiff soil according to NEHRP soil classification. The dataset was compiled from prior studies on seismic analyses of concrete gravity dams (Lokke and Chopra 2013; Zhang et al. 2013; Huang 2014; Toikka et al. 2019; Wang et al. 2017), and assessments of various structures under main shock-aftershock events (Li et al. 2014; Khanal 2019; Mangalathu et al. 2019).

Seismic performance of concrete gravity dams was evaluated using 14 selected main shock-aftershock events (Table A2), with main shock fault distances (R) of 0–19.5 km and magnitudes (M) of 6.0–7.6, and corresponding aftershock distances (R) of 3.4–25 km and magnitudes (M) of 5.3–6.2. Shear wave velocities ($V_{s,30}$) were greater than 382 m/s, with the minimum value corresponding to very dense soil/soft rock per NEHRP soil classification.

Table 1. The first three frequencies of dam-reservoir systems.

	Model I	Model II	Model III
f_1 (Hz)	6.1	3.1	2.1
f_2 (Hz)	13.8	7.5	5.3
f_3 (Hz)	19.6	11.1	7.6

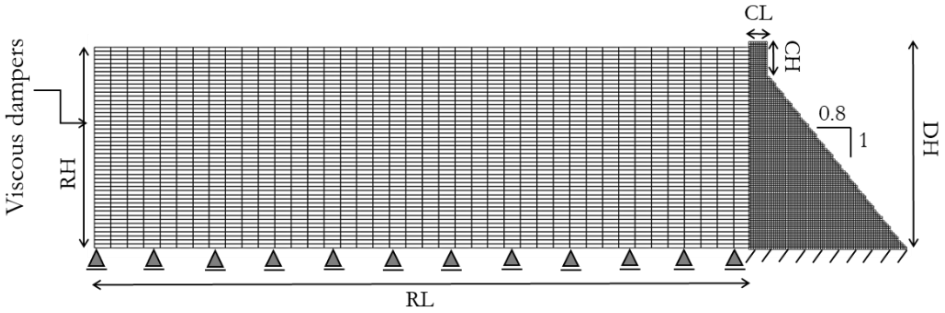

	Model I	Model II	Model III
DH (m)	50	100	150
CL (m)	4	8	12
CH (m)	8	15	20
RL (m)	160	320	456
RH (m)	48	98	148

Fig. 3. Coupled dam-reservoir systems.

5. The Estimation of the Required Time Interval Between Main Shocks and Aftershocks for Concrete Gravity Dams

Many aftershocks occur after a main shock, causing further damage to structures, especially if the damage is not repaired. These aftershocks typically occur after a time interval, allowing the structure to come to rest before the subsequent seismic event. Consequently, in numerical modeling, it is crucial to apply aftershocks once the structure has returned to a stable, resting state. This requires defining an appropriate time interval between successive seismic events. For dams, this time interval has been assumed as fixed values, ranging from 10 seconds (Pang et al. 2019; Wang et al. 2017, 2020; Zhang et al. 2019, 2021; Zhai et al. 2022; Ashna et al. 2024) to 100 seconds (Zhang et al. 2013).

This section proposes empirical rest time equations between main shocks and aftershocks specifically for concrete gravity dam-reservoir systems to reduce computational analysis time in numerical simulations, while ensuring the structure is at rest before the subsequent event. To this end, the three dam-reservoir systems shown in Fig. 3 were subjected to the 124 as-recorded ground motions (Table A1). After each motion, a zero-acceleration period was introduced to determine the time required for the dams to return to a resting state. Following Pirooz et al. (2021), the dams are considered at rest when the free vibration velocity of their crest is ≤0.1% of the maximum free vibration velocity.

Fig. 4 presents the horizontal PGA component versus the normalized rest time (NRT), defined as the estimated rest time divided by the corresponding horizontal PGA component of the ground motion, for the three dam-reservoir systems. A clear nonlinear correlation between NRT and PGA is evident for all models, with Model I (50 m height) showing the lowest NRT, and Model III (150 m height) showing the highest. The natural frequency decreases as the dam height increases, leading to longer rest times. For Models I and III, the rest times ranged from 2.2-3.5 s and 4.6-6.7 s, respectively.

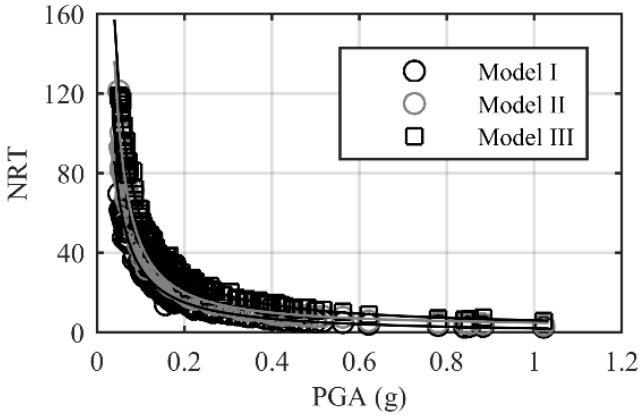

Fig. 4. Normalized rest time (NRT) for concrete gravity dam-reservoir systems.

For the scatter data presented in Fig. 4, a nonlinear curve of the form $y = ax^b + c$ was fitted using the nonlinear least squares method (indicated by solid lines in Fig. 4). The proposed equations for the required time interval between main shock and aftershocks, denoted as NRT_{fitted}, are given in Eqs. (5–7), for Models I-III, respectively.

$$NRT_{\text{fitted,Model I}} = 2.9358PGA^{-1.0502} - 0.9129 \quad (5)$$

$$NRT_{\text{fitted,Model II}} = 2.2684PGA^{-1.2651} + 2.6195 \quad (6)$$

$$NRT_{\text{fitted,Model III}} = 4.3935PGA^{-1.1066} + 1.6151 \quad (7)$$

It should be noted that these equations are based on empirical regression of 124 as-recorded ground motions, specifically derived for concrete gravity dam-reservoir systems with PGAs ranging from 0.05g to 1.02g and dam heights of 50–150 m, with 5% Rayleigh damping. They may not be generalized to other dam types, geometries, or damping ratios without further validation.

6. Seismic Performance Evaluation of Concrete Gravity Dam-Reservoir Systems under Main Shock-Aftershock Events

This section investigates the seismic performances of three concrete gravity dam-reservoir systems with varying heights (Model I – 50 m, Model II – 100 m, Model III – 150 m) under 14 as-recorded main shock-aftershock (MS-AS) earthquake sequences (Table A2). It also evaluates the influence of MS-AS ground motion properties on structural damage to identify the characteristics of damaging AS on concrete gravity dams. The time interval between each sequence was determined using Eqs. (5–7) for the three models. The discrete modeling of the dam body enabled damage assessment through three discrete damage measures: base crack length, maximum base crack width, and maximum total crack width on the upstream (U/S) face.

Four analysis sets were performed. In the first, the Peak Ground Acceleration (PGA) of MS was scaled to 0.5g to ensure nonlinear behavior (Wang et al. 2020), and the same scaling factor was subsequently applied to the corresponding AS. Scaling factors ranged from 0.6 to 4.1 and were uniformly applied to both horizontal and vertical components. In the subsequent sets, the MS PGA was fixed at 0.5g, while the AS PGA was varied at 0.3g, 0.4g, and 0.5g to reflect the observed variability of aftershock intensities in real events (Wang et al. 2017; Guo et al. 2020).

6.1. Damage to concrete gravity dam-reservoir systems for the same scaling factor

Damage indices were computed directly as ratios of MS-AS to MS-only results for each earthquake record (EQ#1 to EQ#14), with a value above 1.0 indicating additional damage due to aftershocks (Table 2).

In most cases, AS did not significantly increase base crack length or width, except Model I, which showed an 11% increase in base crack length for EQ#13 and a 22% increase in base crack width. For Model I, damage was most pronounced at the base, while upstream cracking remained limited. Increases in maximum total crack width on the U/S face ranged from 4% (Model I–EQ#12: from 14.3 mm to 14.9 mm) to 31% (Model II–EQ#14: from 39 mm to 51.2 mm), as illustrated in Table 2 and Fig. 5.

Table 2. Damage measure ratios of MS-AS to MS-only for the same scaling factor of MS-AS.

Model I														
	EQ#1	EQ#2	EQ#3	EQ#4	EQ#5	EQ#6	EQ#7	EQ#8	EQ#9	EQ#10	EQ#11	EQ#12	EQ#13	EQ#14
Base Cr. Length	1.00	1.00	1.00	1.00	1.00	1.00	1.00	1.00	1.00	1.00	1.00	1.00	1.11	1.00
Base Cr. Width	1.00	1.00	1.00	1.00	1.00	1.00	1.00	1.00	1.00	1.00	1.00	1.00	1.22	1.00
U/S Crack Width	1.00	1.00	1.00	1.00	1.00	1.00	1.00	1.00	1.00	1.00	1.01	1.04	1.12	1.06
Model II														
	EQ#1	EQ#2	EQ#3	EQ#4	EQ#5	EQ#6	EQ#7	EQ#8	EQ#9	EQ#10	EQ#11	EQ#12	EQ#13	EQ#14
Base Cr. Length	1.00	1.00	1.00	1.00	1.00	1.00	1.00	1.00	1.00	1.00	1.00	1.00	1.00	1.00
Base Cr. Width	1.00	1.00	1.00	1.00	1.00	1.00	1.00	1.00	1.00	1.00	1.00	1.00	1.00	1.00
U/S Crack Width	1.00	1.00	1.00	1.00	1.00	1.00	1.00	1.00	1.00	1.00	1.01	1.04	1.10	1.31
Model III														
	EQ#1	EQ#2	EQ#3	EQ#4	EQ#5	EQ#6	EQ#7	EQ#8	EQ#9	EQ#10	EQ#11	EQ#12	EQ#13	EQ#14
Base Cr. Length	1.00	1.00	1.00	1.00	1.00	1.00	1.00	1.00	1.00	1.00	1.00	1.03	1.00	1.00
Base Cr. Width	1.00	1.00	1.00	1.00	1.00	1.00	1.00	1.00	1.00	1.00	1.00	1.00	1.00	1.00
U/S Crack Width	1.00	1.00	1.00	1.00	1.00	1.00	1.00	1.00	1.00	1.00	1.10	1.07	1.01	1.00

A closer inspection of crack evolution reveals the mechanical basis of the damage patterns. Aftershocks primarily propagated existing cracks, facilitated by stress concentrations formed at the crack tips during the main shock. The arrival of aftershock seismic waves intensified these stresses at vulnerable zones, further widening and extending the cracks. This effect was most pronounced in Model I, where base cracks exhibited the greatest widening in zones of maximum tensile stress.

While propagation was the dominant mechanism, some new cracks also formed. In Models II and III, several new cracks at the neck and along the upstream face, below the neck region, developed. This indicates that taller dams, influenced by higher vibration modes and reservoir hydrodynamic pressures, can experience crack initiation at multiple elevations, resulting in a more complex damage pattern (Wang et al. 2018).

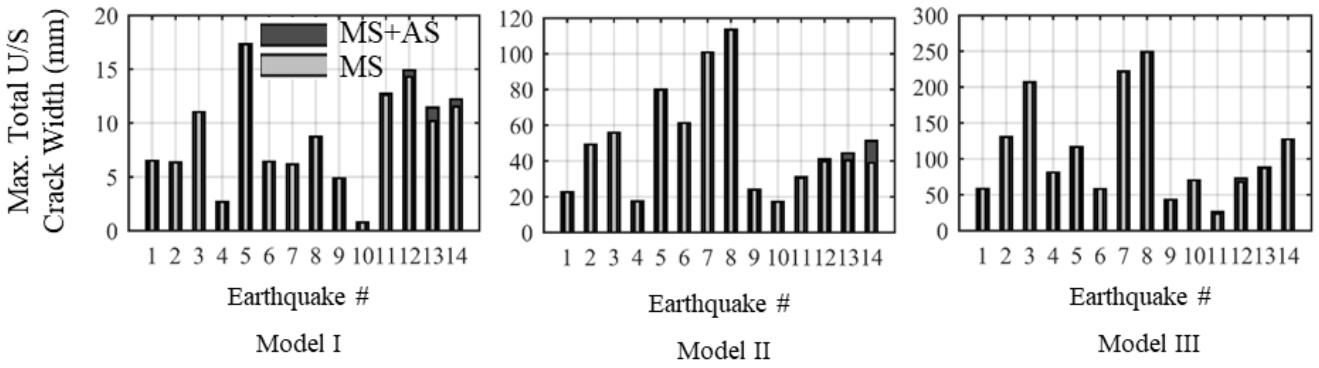

Fig. 5. Maximum total U/S crack width results of dam-reservoir systems under MS-only and MS-AS sequence.

6.2. Damage to concrete gravity dam-reservoir systems under different seismicity levels

Extending the previous analyses, the seismic performance of the three dam-reservoir systems was further evaluated by keeping the main shock (MS) PGA constant at 0.5g while varying the aftershock (AS) PGA to 0.3g, 0.4g, and 0.5g. This approach enabled assessment of crack initiation and propagation while also addressing seepage-related implications for hydraulic safety and dam operation across different AS scenarios. In addition to evaluating overall damage measure ratios, the maximum opening of base cracks and individual U/S cracks was examined for each earthquake record to more precisely assess structural severity and hydraulic implications. The severity of simulated cracks was quantified using the RILEM TC 104 (1991) classification for non-reinforced concrete, in which crack widths are categorized as very mild (<1 mm), mild (1–10 mm), moderate (10–20 mm), and severe (20–25 mm).

The ratios of MS-AS to MS-only damage measure indices are presented in Tables 3-5 for Models I-III, respectively. At 0.3g–0.4g AS intensities, aftershocks generally widened existing U/S cracks or initiated new ones, with limited extension of base cracks. For instance, in Model I, the maximum total crack width on the U/S face increased by 29% at 0.4g (EQ#2: from 6.3 mm to 8.1 mm, Table 3). In Model II, it increased by 20% for EQ#2 (from 45.8 mm to 55.1 mm) and by 30% for EQ#14 (from 39.0 mm to 50.7 mm) (Table 4). In Model III, the maximum total crack width on the U/S face increased by 67% at 0.4g (EQ#11: from 23.6 mm to 39.5 mm, Table 5). A notable case was observed in Model I (EQ#10 at 0.4g) for the base cracks: here, the maximum base crack width increased by 96%, and the crack length extended by 50%. This occurred because the MS produced only a single crack at the base, while the AS both extended it and initiated new cracks at the neck, resulting in a substantial increase in all damage measures.

At 0.5g, new upstream cracks became more frequent, particularly in taller dams. For Model I (EQ#2), the maximum total crack width on the U/S face doubled (from 6.3 mm to 12.7 mm), entirely from the propagation of existing cracks. In Model II, the width increased by 78% (from 45.8 mm to 81.5 mm) due to both new crack formation and propagation of existing cracks. EQ#11 in Model III showed a 2.4-fold increase (from 23.6 mm to 56.8 mm), mainly from new cracks below the neck. The evolution of U/S crack widths with increasing AS intensity is illustrated in Fig. 6. On average, excluding outliers, the maximum total crack width on the U/S face increased by approximately 25–30% at 0.5g AS PGA across all models.

Overall, at 0.3–0.4g AS intensities, aftershocks primarily propagated existing U/S cracks, with occasional base crack extension. At 0.5g, they initiated new cracks at different elevations, creating a more complex damage pattern, especially in taller dams, consistent with the findings of the previous section. Model I highlights neck cracks as critical vulnerabilities. Models II and III show that taller dams are more susceptible to complex AS-induced responses driven by higher modes and reservoir hydrodynamic pressures, which create new tensile stress fields beyond the initial crack zones (Wang et al. 2018).

Applying the RILEM TC 104 (1991) classification, due to the maximum opening of a single crack, Model I consistently remained in the mild category, suggesting a robust safety margin. Models II and III exhibited similar responses: mild damage was dominant for many events, while several records produced moderate cracks both at the base and U/S regions, indicating higher sensitivity to seismic effects. These findings emphasize practical implications for dam operations and safety. Smaller dams maintain stable performance with minimal risk to dam functionality. In contrast, taller dams (Models II and III) are more vulnerable to U/S cracking and seepage, often accompanied by more distributed damage patterns. Because cracks in the upstream face are in direct contact with reservoir water, they may compromise hydraulic safety by facilitating seepage, which can accelerate internal erosion or induce localized instability (Pekau and Zhu 2008). Even moderate U/S crack widths may therefore have significant implications for dam safety and operational management, necessitating careful monitoring, possible mitigation measures, and explicit consideration of aftershocks in design checks and emergency operation planning.

6.3. The effect of ground motion properties on the damage to concrete gravity dam-reservoir systems

Following the findings in the preceding section, it is evident that aftershocks can significantly increase damage to dam-reservoir systems, ranging from minor per-

centages to over 200%. To better understand this phenomenon, a comprehensive study explored how specific ground motion characteristics contribute to additional damage. Although over 25 intensity measures (IMs) were examined, this section presents only the results for Arias Intensity, sustained maximum acceleration, effective design acceleration (EDA), and damage index to maintain conciseness.

Table 3. Damage measure ratios of MS-AS to MS-only under different seismicity levels for Model I.

MS PGA: 0.5g – AS PGA: 0.3g														
	EQ#1	EQ#2	EQ#3	EQ#4	EQ#5	EQ#6	EQ#7	EQ#8	EQ#9	EQ#10	EQ#11	EQ#12	EQ#13	EQ#14
Base Cr. Length	1.00	1.00	1.00	1.00	1.00	1.00	1.00	1.00	1.00	1.07	1.00	1.00	1.00	1.00
Base Cr. Width	1.00	1.00	1.00	1.00	1.00	1.00	1.00	1.00	1.00	1.18	1.00	1.00	1.00	1.00
U/S Crack Width	1.00	1.00	1.00	1.00	1.00	1.00	1.00	1.00	1.00	5.80	1.01	1.00	1.00	1.00
MS PGA: 0.5g – AS PGA: 0.4g														
	EQ#1	EQ#2	EQ#3	EQ#4	EQ#5	EQ#6	EQ#7	EQ#8	EQ#9	EQ#10	EQ#11	EQ#12	EQ#13	EQ#14
Base Cr. Length	1.00	1.25	1.00	1.00	1.00	1.00	1.13	1.00	1.00	1.50	1.00	1.00	1.00	1.00
Base Cr. Width	1.00	1.07	1.00	1.00	1.00	1.00	1.00	1.00	1.00	1.96	1.00	1.00	1.00	1.00
U/S Crack Width	1.00	1.29	1.00	1.00	1.00	1.00	1.07	1.00	1.09	8.99	1.06	1.03	1.00	1.05
MS PGA: 0.5g – AS PGA: 0.5g														
	EQ#1	EQ#2	EQ#3	EQ#4	EQ#5	EQ#6	EQ#7	EQ#8	EQ#9	EQ#10	EQ#11	EQ#12	EQ#13	EQ#14
Base Cr. Length	1.00	1.73	1.06	1.00	1.03	1.04	1.13	1.02	1.02	2.00	1.00	1.00	1.03	1.07
Base Cr. Width	1.00	2.81	1.03	1.16	1.00	1.00	1.00	1.06	1.00	3.00	1.00	1.00	1.00	1.00
U/S Crack Width	1.00	2.01	1.13	1.23	1.04	1.03	1.95	1.02	1.32	14.48	1.17	1.07	1.00	1.10

Table 4. Damage measure ratios of MS-AS to MS-only under different seismicity levels for Model II.

MS PGA: 0.5g – AS PGA: 0.3g														
	EQ#1	EQ#2	EQ#3	EQ#4	EQ#5	EQ#6	EQ#7	EQ#8	EQ#9	EQ#10	EQ#11	EQ#12	EQ#13	EQ#14
Base Cr. Length	1.00	1.00	1.00	1.00	1.00	1.00	1.00	1.00	1.00	1.00	1.00	1.00	1.00	1.00
Base Cr. Width	1.00	1.00	1.00	1.00	1.00	1.00	1.00	1.00	1.00	1.00	1.00	1.00	1.00	1.00
U/S Crack Width	1.00	1.04	1.00	1.00	1.00	1.00	1.00	1.00	1.00	1.00	1.02	1.00	1.00	1.00
MS PGA: 0.5g – AS PGA: 0.4g														
	EQ#1	EQ#2	EQ#3	EQ#4	EQ#5	EQ#6	EQ#7	EQ#8	EQ#9	EQ#10	EQ#11	EQ#12	EQ#13	EQ#14
Base Cr. Length	1.00	1.02	1.00	1.03	1.00	1.00	1.00	1.00	1.00	1.10	1.05	1.00	1.00	1.00
Base Cr. Width	1.00	1.13	1.00	1.00	1.00	1.00	1.00	1.00	1.00	1.25	1.00	1.00	1.00	1.00
U/S Crack Width	1.00	1.20	1.05	1.10	1.01	1.03	1.00	1.02	1.21	1.26	1.06	1.01	1.00	1.30
MS PGA: 0.5g – AS PGA: 0.5g														
	EQ#1	EQ#2	EQ#3	EQ#4	EQ#5	EQ#6	EQ#7	EQ#8	EQ#9	EQ#10	EQ#11	EQ#12	EQ#13	EQ#14
Base Cr. Length	1.00	1.19	1.00	1.10	1.00	1.02	1.00	1.00	1.00	1.19	1.19	1.00	1.00	1.00
Base Cr. Width	1.00	1.10	1.00	1.00	1.00	1.00	1.00	1.00	1.00	1.49	1.18	1.00	1.00	1.00
U/S Crack Width	1.02	1.78	1.16	1.72	1.03	1.10	1.02	1.04	1.54	2.15	1.17	1.10	1.00	1.45

Table 5. Damage measure ratios of MS-AS to MS-only under different seismicity levels for Model III.

	EQ#1	EQ#2	EQ#3	EQ#4	EQ#5	EQ#6	EQ#7	EQ#8	EQ#9	EQ#10	EQ#11	EQ#12	EQ#13	EQ#14
MS PGA: 0.5g – AS PGA: 0.3g														
Base Cr. Length	1.00	1.01	1.00	1.01	1.00	1.00	1.00	1.00	1.00	1.00	1.00	1.00	1.00	1.00
Base Cr. Width	1.00	1.00	1.00	1.00	1.00	1.00	1.00	1.00	1.00	1.00	1.00	1.00	1.00	1.00
U/S Crack Width	1.00	1.02	1.00	1.05	1.00	1.00	1.03	1.00	1.02	1.00	1.10	1.02	1.00	1.00
MS PGA: 0.5g – AS PGA: 0.4g														
	EQ#1	EQ#2	EQ#3	EQ#4	EQ#5	EQ#6	EQ#7	EQ#8	EQ#9	EQ#10	EQ#11	EQ#12	EQ#13	EQ#14
Base Cr. Length	1.00	1.12	1.00	1.10	1.00	1.00	1.00	1.00	1.02	1.02	1.00	1.01	1.00	1.00
Base Cr. Width	1.00	1.18	1.00	1.06	1.00	1.00	1.00	1.00	1.00	1.00	1.00	1.00	1.00	1.00
U/S Crack Width	1.00	1.25	1.00	1.28	1.00	1.00	1.09	1.00	1.38	1.18	1.67	1.06	1.00	1.00
MS PGA: 0.5g – AS PGA: 0.5g														
	EQ#1	EQ#2	EQ#3	EQ#4	EQ#5	EQ#6	EQ#7	EQ#8	EQ#9	EQ#10	EQ#11	EQ#12	EQ#13	EQ#14
Base Cr. Length	1.00	1.22	1.00	1.23	1.00	1.04	1.00	1.00	1.09	1.08	1.04	1.07	1.00	1.00
Base Cr. Width	1.00	1.35	1.00	1.31	1.00	1.00	1.00	1.00	1.03	1.00	1.01	1.09	1.00	1.00
U/S Crack Width	1.00	1.61	1.02	1.71	1.01	1.01	1.26	1.01	1.76	1.56	2.41	1.18	1.01	1.00

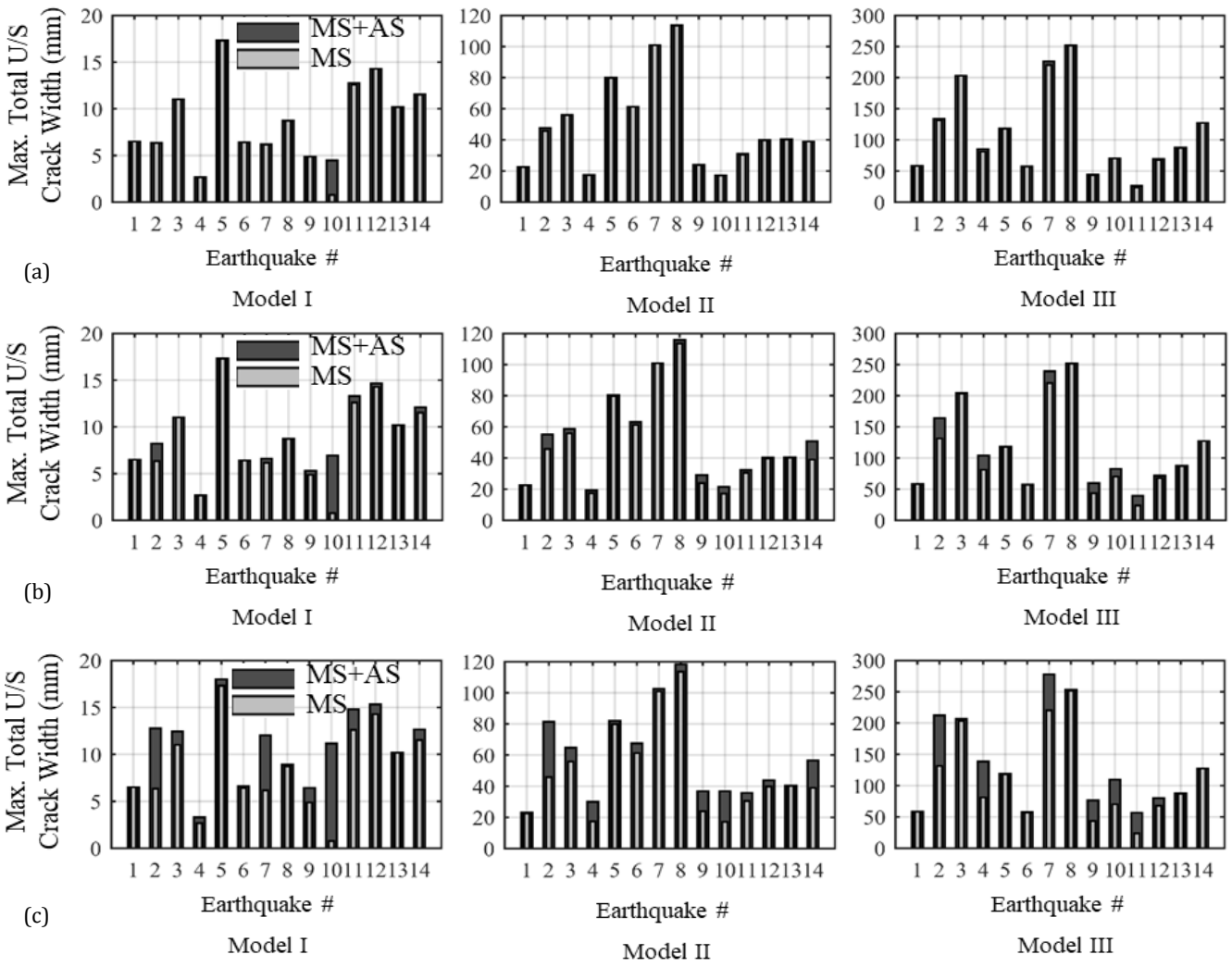

Fig. 6. Maximum total U/S crack width results of dam-reservoir systems under MS-only and under different seismicity levels of MS-AS sequence: (a) MS PGA: 0.5g – AS PGA: 0.3g; (b) MS PGA: 0.5g – AS PGA: 0.4g; (c) MS PGA: 0.5g – AS PGA: 0.5g.

Fig. 7 illustrates the influence of selected ground motion IMs on the increase of the maximum total crack width on the U/S face for the 0.5g AS case. In this figure, the horizontal axis represents the ratio of AS-to-MS intensity measures, while the vertical axis shows the ratio of maximum total crack width on the U/S face for MS–AS sequences to that for MS-only events. A ratio above 1.0 on the y-axis indicates that the aftershock caused additional damage in terms of U/S crack width. Outlier data from EQ#10 in Model I are excluded from the plots to reveal the overall trends better.

For Arias Intensity (Fig. 7(a)), in Model I, AS increased U/S crack widths when the AS-to-MS intensity measure ratio exceeded 0.34. This threshold was lower for Models II and III, at 0.28. In total, 39 out of 42 sequences across all models showed further damage when the Arias Intensity ratio exceeded 0.27.

Sustained maximum acceleration (Fig. 7(b)) showed a similar pattern. For Model I, U/S cracks widened further when the AS-to-MS intensity measure ratio exceeded 0.46; for Models II and III, this threshold was lower at 0.38. Again, 39 of the 42 MS-AS sequences across the three models resulted in additional U/S damage when the sustained maximum acceleration ratio exceeded 0.37.

In the case of effective design acceleration (EDA) (Fig. 7(c)), the threshold for increased U/S crack widths in Model I was an AS-to-MS intensity measure ratio of 0.95. For Models II and III, the thresholds were 0.86. When the EDA ratio exceeded 0.85, further U/S cracking was observed in 39 of the 42 earthquake sequences.

Lastly, for the damage index (Fig. 7(d)), the threshold AS-to-MS intensity measure ratio across all dam models was 0.28. As with the other IMs, 39 of the 42 sequences led to increased U/S crack widths when the damage index ratio exceeded 0.26.

The uncertainty of the reported threshold values was quantified by applying a non-parametric bootstrapping method (Mooney and Duval 1993). Using 10000 resamples with replacement, the 95% Confidence Intervals for Arias Intensity, sustained maximum acceleration, EDA, and damage index were computed as [0.27-0.45], [0.37-0.73], [0.85-0.96], and [0.26-0.40], respectively. These damage thresholds are intended for use with concrete gravity dams 50–150 m in height, under MS–AS sequences where both PGAs are scaled to 0.5g with 5% Rayleigh damping. They may not be directly extended to other dam types, geometries, damping ratios, or seismic intensity ranges without further validation. Given the small sample size (14 cases), these values should be regarded as empirical indicators, with larger datasets needed for rigorous statistical inference.

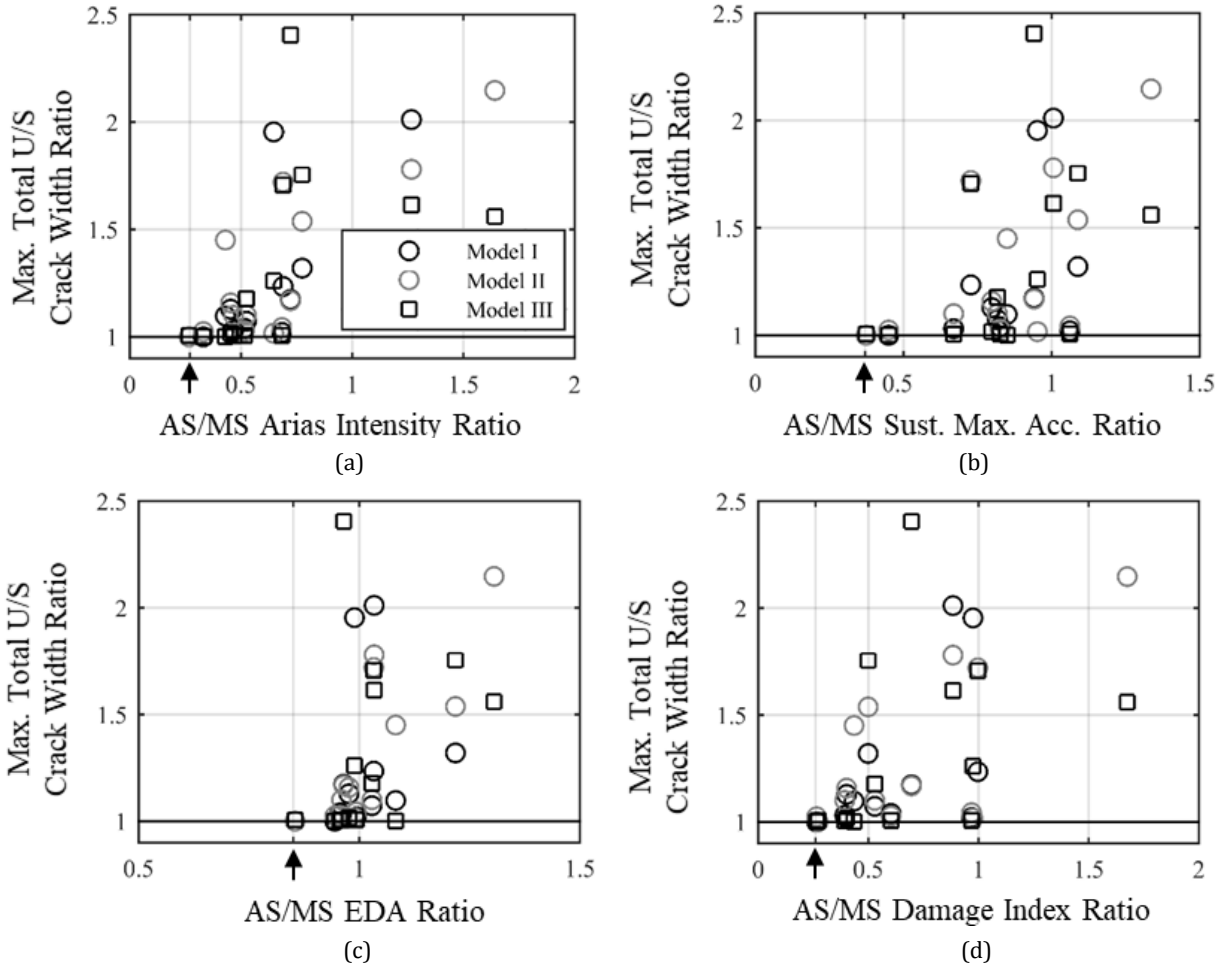

Fig. 7. Ground motion intensity measures on the damage to concrete gravity dam-reservoir systems for 0.5g scaled AS PGA: (a) Arias Intensity; (b) Sustained maximum acceleration; (c) Effective design acceleration; (d) Damage index.

7. Conclusions

This study investigated the seismic performance of three concrete gravity dam-reservoir systems (Model I – 50 m, Model II – 100 m, Model III – 150 m) under as-recorded main shock–aftershock (MS–AS) earthquake sequences using the Modified Applied Element Method (MAEM). Horizontal and vertical components of ground motions were applied in nonlinear transient analyses, and damage was quantified using discrete measures of base crack length, maximum base crack width, and maximum total crack width on the upstream (U/S) face. The use of MAEM provided mechanistic insight into how aftershocks influenced crack patterns and damage accumulation in concrete gravity dams, thereby addressing dam safety.

The results obtained in this study are summarized as follows:

- The rest times between MS-AS sequences ranged from 2.2 to 6.7 s. As the dam height increases, the natural frequency decreases, requiring longer times for taller dams. The empirical Eqs. (5–7) predict these rest times for dams with 50-150 m heights under a PGA range of 0.05g-1.02g with 5% Rayleigh damping.
- Under the same scaling factor, AS primarily propagated existing cracks through stress concentrations formed at crack tips, which was most evident at the base of Model I. In taller dams, in addition to propagation, new cracks developed along the upstream face due to the effects of higher vibration modes and hydrodynamic pressures.
- At 0.3g–0.4g AS intensities, AS generally widened existing upstream cracks or initiated new ones, with limited extension of base cracks. New upstream cracks became more frequent at 0.5g intensity, especially in taller dams. At this seismicity level, the AS increased the maximum total crack width on the upstream face by approximately 25–30% on average, across all models.
- The evaluation of the severity of cracks according to RILEM TC 104 (1991) classification revealed that Model I remained within the mild category across all cases, while Models II and III occasionally reached moderate damage levels both at the base and upstream regions. Since the upstream cracks are in direct contact with the reservoir, they may pose direct hydraulic safety risks. Therefore, even moderate crack openings may increase the potential for seepage, internal erosion, or localized instability, thereby compromising dam functionality.
- A 93% probability was observed for increased maximum total crack width on the upstream face in the three dam systems when the ratios of 0.5g scaled AS to 0.5g scaled MS exceeded 0.27 for Arias Intensity, 0.37 for sustained maximum acceleration, 0.85 for effective design acceleration, and 0.26 for damage index. 95% Confidence Intervals were determined using 10000 bootstrap resamples: [0.27–0.45] for Arias Intensity, [0.37–0.73] for sustained maximum acceleration, [0.85–0.96] for effective design acceleration, and [0.26–0.40] for damage index. These threshold intervals are empirical, with larger datasets needed for rigorous statistical inference.

With a focus on assessing cracking on dam bodies, the soil-structure interaction was not modeled; therefore, the results are applicable for monoliths on stiff foundations (i.e., foundation moduli, E_f, over structure moduli, E_s, more than 4), or for monoliths in narrow valleys with $E_f/E_s < 2$ (Bybordiani and Arici 2017).

This study demonstrates that aftershocks can significantly amplify damage in concrete gravity dams, particularly in taller dams, through combined crack propagation and initiation mechanisms. The findings provide guidance for assessing dam vulnerability, prioritizing inspections, evaluating hydraulic risks from upstream cracking, and incorporating sequential seismic events into design and emergency planning.

Appendix A. Selected earthquake ground motions

The selected 124 acceleration records for the estimation of the required time interval between main shocks and aftershocks are presented in Table A1.

Table A1. Selected earthquake motions.

#	Year	Event	Station	Comp	Mag	R (km)	PGA (g)
1	1966	Parkfield	Cholame Shandon Array	50	6.2 (M_w)	17.6	0.06
2	1966	Parkfield	Cholame Shandon Array	320	6.2 (M_w)	17.6	0.06
3	1971	San Fernando	LA - Hollywood Stor FF	90	6.6 (M_w)	22.8	0.22
4	1971	San Fernando	LA - Hollywood Stor FF	180	6.6 (M_w)	22.8	0.19
5	1971	San Fernando	Lake Hughes 4	111	6.6 (M_w)	19.5	0.20
6	1971	San Fernando	Lake Hughes 4	201	6.6 (M_w)	19.5	0.16
7	1979	Imperial Valley-06	Agrarias	3	6.5 (M_w)	0.0	0.29
8	1979	Imperial Valley-06	Agrarias	273	6.5 (M_w)	0.0	0.19
9	1979	Imperial Valley-06	El Centro Array 7	140	6.5 (M_w)	0.6	0.34
10	1979	Imperial Valley-06	El Centro Array 7	230	6.5 (M_w)	0.6	0.47
11	1979	Imperial Valley-06	Holtville Post Office	225	6.5 (M_w)	5.4	0.26

12	1979	Imperial Valley-06	Holtville Post Office	315	6.5 (M_w)	5.4	0.22
13	1979	Imperial Valley-06	Victoria	75	6.5 (M_w)	31.9	0.12
14	1979	Imperial Valley-06	Victoria	345	6.5 (M_w)	31.9	0.17
15	1980	Mammoth Lakes-01	Long Valley Dam (Upr L Abut)	0	6.1 (M_w)	12.6	0.43
16	1980	Mammoth Lakes-01	Long Valley Dam (Upr L Abut)	90	6.1 (M_w)	12.6	0.27
17	1980	Mammoth Lakes-01	Mammoth Lakes H. S.	254	6.1 (M_w)	4.5	0.32
18	1980	Mammoth Lakes-01	Mammoth Lakes H. S.	344	6.1 (M_w)	4.5	0.24
19	1980	Mammoth Lakes-02	Long Valley Dam (Upr L Abut)	0	5.7 (M_w)	14.3	0.19
20	1980	Mammoth Lakes-02	Long Valley Dam (Upr L Abut)	90	5.7 (M_w)	14.3	0.07
21	1980	Irpinia, Italy-01	Auletta	0	6.9 (M_w)	9.5	0.06
22	1980	Irpinia, Italy-01	Auletta	270	6.9 (M_w)	9.5	0.06
23	1980	Irpinia, Italy-01	Bagnoli Irpinio	0	6.9 (M_w)	8.1	0.13
24	1980	Irpinia, Italy-01	Bagnoli Irpinio	270	6.9 (M_w)	8.1	0.19
25	1980	Irpinia, Italy-01	Brienza	0	6.9 (M_w)	22.5	0.22
26	1980	Irpinia, Italy-01	Brienza	270	6.9 (M_w)	22.5	0.18
27	1980	Irpinia, Italy-01	Rionero In Vulture	0	6.9 (M_w)	27.5	0.10
28	1980	Irpinia, Italy-01	Rionero In Vulture	270	6.9 (M_w)	27.5	0.10
29	1980	Irpinia, Italy-02	Bagnoli Irpinio	0	6.2 (M_w)	17.8	0.06
30	1980	Irpinia, Italy-02	Bagnoli Irpinio	270	6.2 (M_w)	17.8	0.05
31	1983	Mammoth Lakes-11	Convict Creek	90	5.3 (M_w)	7.1	0.15
32	1983	Mammoth Lakes-11	Convict Creek	180	5.3 (M_w)	7.1	0.09
33	1983	Coalinga-05	Oil City	270	5.8 (M_w)	2.0	0.84
34	1983	Coalinga-05	Oil City	360	5.8 (M_w)	2.0	0.42
35	1983	Coalinga-05	Oil Fields Fire Station - FF	270	5.8 (M_w)	6.3	0.22
36	1983	Coalinga-05	Oil Fields Fire Station - FF	360	5.8 (M_w)	6.3	0.19
37	1983	Coalinga-05	Transmitter Hill	270	5.8 (M_w)	3.7	0.78
38	1983	Coalinga-05	Transmitter Hill	360	5.8 (M_w)	3.7	1.02
39	1984	Morgan Hill	Gilroy Array 2	0	6.2 (M_w)	13.7	0.16
40	1984	Morgan Hill	Gilroy Array 2	90	6.2 (M_w)	13.7	0.21
41	1986	N. Palm Springs	San Jacinto - Valley Cemetary	270	6.1 (M_w)	30.7	0.07
42	1986	N. Palm Springs	San Jacinto - Valley Cemetary	360	6.1 (M_w)	30.7	0.06
43	1986	N. Palm Springs	Sunnymead	225	6.1 (M_w)	37.7	0.10
44	1986	N. Palm Springs	Sunnymead	315	6.1 (M_w)	37.7	0.12
45	1986	Chalfant Valley-02	Benton	270	6.2 (M_w)	21.6	0.21
46	1986	Chalfant Valley-02	Benton	360	6.2 (M_w)	21.6	0.18
47	1986	Chalfant Valley-02	Bishop - Paradise Lodge	70	6.2 (M_w)	15.0	0.17
48	1986	Chalfant Valley-02	Bishop - Paradise Lodge	160	6.2 (M_w)	15.0	0.16
49	1987	Whittier Narrows-01	Alhambra - Fremont School	180	6.0 (M_w)	1.7	0.29
50	1987	Whittier Narrows-01	Alhambra - Fremont School	270	6.0 (M_w)	1.7	0.39
51	1987	Whittier Narrows-01	Glendale - Las Palmas	177	6.0 (M_w)	14.7	0.30
52	1987	Whittier Narrows-01	Glendale - Las Palmas	267	6.0 (M_w)	14.7	0.18
53	1987	Whittier Narrows-01	Glendora - N Oakbank	80	6.0 (M_w)	13.7	0.10
54	1987	Whittier Narrows-01	Glendora - N Oakbank	170	6.0 (M_w)	13.7	0.11
55	1987	Whittier Narrows-01	LA - Century City CC North	0	6.0 (M_w)	26.1	0.07
56	1987	Whittier Narrows-01	LA - Century City CC North	90	6.0 (M_w)	26.1	0.10
57	1987	Whittier Narrows-01	Pasadena - CIT Kresge Lab	90	6.0 (M_w)	6.8	0.11
58	1987	Whittier Narrows-01	Pasadena - CIT Kresge Lab	360	6.0 (M_w)	6.8	0.09
59	1987	Whittier Narrows-01	Pomona - 4th & Locust FF	12	6.0 (M_w)	25.1	0.07
60	1987	Whittier Narrows-01	Pomona - 4th & Locust FF	102	6.0 (M_w)	25.1	0.05

61	1987	Whittier Narrows-02	Alhambra - Fremont School	180	5.3 (M_w)	3.6	0.18
62	1987	Whittier Narrows-02	Alhambra - Fremont School	270	5.3 (M_w)	3.6	0.21
63	1987	Whittier Narrows-02	LA - Hollywood Stor FF	90	5.3 (M_w)	21.0	0.05
64	1987	Whittier Narrows-02	LA - Hollywood Stor FF	360	5.3 (M_w)	21.0	0.09
65	1989	Loma Prieta	Point Bonita	207	6.9 (M_w)	83.4	0.07
66	1989	Loma Prieta	Point Bonita	297	6.9 (M_w)	83.4	0.07
67	1989	Loma Prieta	So. San Francisco, Sierra Pt.	115	6.9 (M_w)	63.0	0.05
68	1989	Loma Prieta	So. San Francisco, Sierra Pt.	205	6.9 (M_w)	63.0	0.11
69	1992	Landers	Mission Creek Fault	0	7.3 (M_w)	27.0	0.13
70	1992	Landers	Mission Creek Fault	90	7.3 (M_w)	27.0	0.13
71	1994	Northridge-01	Beverly Hills - 12520 Mulhol	35	6.7 (M_w)	12.4	0.62
72	1994	Northridge-01	Beverly Hills - 12520 Mulhol	125	6.7 (M_w)	12.4	0.45
73	1994	Northridge-01	Burbank - Howard Rd.	60	6.7 (M_w)	15.9	0.11
74	1994	Northridge-01	Burbank - Howard Rd.	330	6.7 (M_w)	15.9	0.16
75	1994	Northridge-01	LA - Centinela St	155	6.7 (M_w)	20.4	0.45
76	1994	Northridge-01	LA - Centinela St	245	6.7 (M_w)	20.4	0.32
77	1994	Northridge-01	LA - Obregon Park	90	6.7 (M_w)	35.4	0.35
78	1994	Northridge-01	LA - Obregon Park	360	6.7 (M_w)	35.4	0.56
79	1994	Northridge-01	LA - Wonderland Ave	95	6.7 (M_w)	15.1	0.10
80	1994	Northridge-01	LA - Wonderland Ave	185	6.7 (M_w)	15.1	0.16
81	1994	Northridge-01	LA 00	180	6.7 (M_w)	9.9	0.26
82	1994	Northridge-01	LA 00	270	6.7 (M_w)	9.9	0.38
83	1994	Northridge-01	Lake Hughes 12A	90	6.7 (M_w)	20.8	0.17
84	1994	Northridge-01	Lake Hughes 12A	180	6.7 (M_w)	20.8	0.26
85	1994	Northridge-01	Santa Monica City Hall	90	6.7 (M_w)	17.3	0.88
86	1994	Northridge-01	Santa Monica City Hall	360	6.7 (M_w)	17.3	0.37
87	1994	Northridge-01	Sylmar - Converter Sta East	11	6.7 (M_w)	0.0	0.85
88	1994	Northridge-01	Sylmar - Converter Sta East	281	6.7 (M_w)	0.0	0.45
89	1999	Kocaeli, Turkey	Arcelik	0	7.5 (M_w)	10.6	0.21
90	1999	Kocaeli, Turkey	Arcelik	90	7.5 (M_w)	10.6	0.13
91	1999	Chi-Chi, Taiwan	CHY035	E	7.6 (M_w)	12.6	0.25
92	1999	Chi-Chi, Taiwan	CHY035	N	7.6 (M_w)	12.6	0.25
93	1999	Chi-Chi, Taiwan	CHY042	E	7.6 (M_w)	27.5	0.10
94	1999	Chi-Chi, Taiwan	CHY042	N	7.6 (M_w)	27.5	0.07
95	1999	Chi-Chi, Taiwan	CHY052	N	7.6 (M_w)	38.7	0.15
96	1999	Chi-Chi, Taiwan	CHY052	W	7.6 (M_w)	38.7	0.09
97	1999	Hector Mine	Twentynine Palms	90	7.1 (M_w)	42.1	0.07
98	1999	Hector Mine	Twentynine Palms	360	7.1 (M_w)	42.1	0.07
99	1999	Chi-Chi, Taiwan-03	TCU079	E	6.2 (M_w)	0.0	0.34
100	1999	Chi-Chi, Taiwan-03	TCU079	N	6.2 (M_w)	0.0	0.27
101	1999	Chi-Chi, Taiwan-04	CHY035	E	6.2 (M_w)	25.0	0.13
102	1999	Chi-Chi, Taiwan-04	CHY035	N	6.2 (M_w)	25.0	0.12
103	1999	Chi-Chi, Taiwan-05	TCU054	E	6.2 (M_w)	45.3	0.06
104	1999	Chi-Chi, Taiwan-05	TCU054	N	6.2 (M_w)	45.3	0.05
105	1999	Chi-Chi, Taiwan-06	TCU075	E	6.3 (M_w)	24.3	0.11
106	1999	Chi-Chi, Taiwan-06	TCU075	N	6.3 (M_w)	24.3	0.06
107	1999	Chi-Chi, Taiwan-06	TCU120	E	6.3 (M_w)	30.9	0.06
108	1999	Chi-Chi, Taiwan-06	TCU120	N	6.3 (M_w)	30.9	0.06
109	2009	L'Aquila, Italy	L'Aquila - V. Aterno - Colle Grilli	E	6.3 (M_w)	0.0	0.48

110	2009	L'Aquila, Italy	L'Aquila - V. Aterno - Colle Grilli	N	6.3 (M_w)	0.0	0.52
111	2009	L'Aquila (aftershock 1), Italy	L'Aquila - V. Aterno - Colle Grilli	E	5.6 (M_w)	11.1	0.15
112	2009	L'Aquila (aftershock 1), Italy	L'Aquila - V. Aterno - Colle Grilli	N	5.6 (M_w)	11.1	0.11
113	2008	Iwate, Japan	IWTH17	EW	6.9 (M_w)	72.4	0.06
114	2008	Iwate, Japan	IWTH17	NS	6.9 (M_w)	72.4	0.06
115	2008	Iwate, Japan	MYG011	EW	6.9 (M_w)	82.9	0.06
116	2008	Iwate, Japan	MYG011	NS	6.9 (M_w)	82.9	0.08
117	1995	Kozani, Greece	ITSAK	90	6.1 (M_L)	19.5	0.14
118	1995	Kozani, Greece	ITSAK	90	5.3 (M_L)	12.1	0.12
119	1980	Mammoth Lakes	54099 Convict Creek	90	6.1 (M_L)	9.1	0.41
120	1980	Mammoth Lakes	54099 Convict Creek	90	5.7 (M_L)	3.4	0.35
121	1995	Kozani, Greece	ITSAK	0	6.1 (M_L)	19.5	0.22
122	1995	Kozani, Greece	ITSAK	0	5.3 (M_L)	12.1	0.13
123	1980	Mammoth Lakes	54099 Convict Creek	180	6.1 (M_L)	9.1	0.40
124	1980	Mammoth Lakes	54099 Convict Creek	180	5.7 (M_L)	3.4	0.50

The 14 ground motion records to evaluate the seismic performances of concrete gravity dam-reservoir systems are given in Table A2.

Table A2. Selected main shocks-aftershocks.

#	MS/AS	Year	Event	Station	Comp	Mag	R (km)	PGA (g)
1	MS	1980	Mammoth Lakes-01	Long Valley Dam (Upr L Abut)	0	6.1 (M_w)	12.6	0.43
	AS	1980	Mammoth Lakes-02	Long Valley Dam (Upr L Abut)	0	5.7 (M_w)	14.3	0.19
2	MS	1980	Mammoth Lakes-01	Long Valley Dam (Upr L Abut)	90	6.1 (M_w)	12.6	0.27
	AS	1980	Mammoth Lakes-02	Long Valley Dam (Upr L Abut)	90	5.7 (M_w)	14.3	0.07
3	MS	1980	Irpinia, Italy-01	Bagnoli Irpinio	0	6.9 (M_w)	8.1	0.13
	AS	1980	Irpinia, Italy-02	Bagnoli Irpinio	0	6.2 (M_w)	17.8	0.06
4	MS	1980	Irpinia, Italy-01	Bagnoli Irpinio	270	6.9 (M_w)	8.1	0.19
	AS	1980	Irpinia, Italy-02	Bagnoli Irpinio	270	6.2 (M_w)	17.8	0.05
5	MS	1987	Whittier Narrows-01	Alhambra - Fremont School	180	6.0 (M_w)	1.7	0.29
	AS	1987	Whittier Narrows-02	Alhambra - Fremont School	180	5.3 (M_w)	3.6	0.18
6	MS	1987	Whittier Narrows-01	Alhambra - Fremont School	270	6.0 (M_w)	1.7	0.39
	AS	1987	Whittier Narrows-02	Alhambra - Fremont School	270	5.3 (M_w)	3.6	0.21
7	MS	1999	Chi-Chi, Taiwan	CHY035	E	7.6 (M_w)	12.6	0.25
	AS	1999	Chi-Chi, Taiwan-04	CHY035	E	6.2 (M_w)	25.0	0.13
8	MS	1999	Chi-Chi, Taiwan	CHY035	N	7.6 (M_w)	12.6	0.25
	AS	1999	Chi-Chi, Taiwan-04	CHY035	N	6.2 (M_w)	25.0	0.12
9	MS	2009	L'Aquila, Italy	L'Aquila - V. Aterno - Colle Grilli	E	6.3 (M_w)	0.0	0.48
	AS	2009	L'Aquila (aftershock 1), Italy	L'Aquila - V. Aterno - Colle Grilli	E	5.6 (M_w)	11.1	0.15
10	MS	2009	L'Aquila, Italy	L'Aquila - V. Aterno - Colle Grilli	N	6.3 (M_w)	0.0	0.52
	AS	2009	L'Aquila (aftershock 1), Italy	L'Aquila - V. Aterno - Colle Grilli	N	5.6 (M_w)	11.1	0.11
11	MS	1995	Kozani, Greece	ITSAK	0	6.1 (M_L)	19.5	0.22
	AS	1995	Kozani, Greece	ITSAK	0	5.3 (M_L)	12.1	0.13
12	MS	1995	Kozani, Greece	ITSAK	90	6.1 (M_L)	19.5	0.14
	AS	1995	Kozani, Greece	ITSAK	90	5.3 (M_L)	12.1	0.12
13	MS	1980	Mammoth Lakes	54099 Convict Creek	180	6.1 (M_L)	9.1	0.40
	AS	1980	Mammoth Lakes	54099 Convict Creek	180	5.7 (M_L)	3.4	0.50
14	MS	1980	Mammoth Lakes	54099 Convict Creek	90	6.1 (M_L)	9.1	0.41
	AS	1980	Mammoth Lakes	54099 Convict Creek	90	5.7 (M_L)	3.4	0.35

Acknowledgements

None declared.

Funding

The author received no financial support for the research, authorship, and/or publication of this manuscript.

Conflict of Interest

The author declared no potential conflicts of interest with respect to the research, authorship, and/or publication of this manuscript.

Author Contributions

The author confirms sole responsibility for all aspects of the study including conception and design, acquisition of data, analysis and interpretation of data, drafting the manuscript, revising it critically for important intellectual content; and gave final approval of the version to be published.

Data Availability

The datasets created and/or analyzed during the current study are not publicly available, but are available from the corresponding author upon reasonable request.

REFERENCES

Akköse M, Dumanoğlu AA, Bayraktar A (2016). Seismic analysis of arch dams subjected to in-phase and anti-phase ground motions. *Challenge Journal of Structural Mechanics*, 2(2), 85-92.

Akpinar U, Arici Y, Binici B (2023). Post-earthquake effects on the seismic performance of concrete gravity dams. *Structure and Infrastructure Engineering*, 21(1), 10-23.

Alliard PM, Leger P (2008). Earthquake safety evaluation of gravity dams considering aftershocks and reduced drainage efficiency. *Journal of Engineering Mechanics*, 134, 12-22.

Amadio C, Fragiacomo M, Rajgelj S (2003). The effects of repeated earthquake ground motions on the non-linear response of SDOF systems. *Earthquake Engineering & Structural Dynamics*, 32, 291-308.

Ashna KN, Maheshwari P, Viladkar MN (2024). Fragility analysis of a concrete gravity dam under mainshock-aftershock sequences. *Structures*, 61, 106117.

Bybordiani M, Arici Y (2017). The use of 3D modeling for the prediction of the seismic demands on the gravity dams. *Earthquake Engineering & Structural Dynamics*, 46(11), 1769-1789.

Carpinteri A, Valente S, Ferrara G, Imperato L (1992). Experimental and numerical fracture modelling of a gravity dam. *ACI Symposium Publication*, 143, 107-122.

Chen D-H, Yang Z-H, Wang M, Xie J-H (2019). Seismic performance and failure modes of the Jin'anqiao concrete gravity dam based on incremental dynamic analysis. *Engineering Failure Analysis*, 100, 227-244.

Chopra AK (1978). Earthquake resistant design of concrete gravity dams. *Journal of the Structural Division*, 104, 953-971.

Fahlbusch H (2009). Early dams. *Proceedings of the Institution of Civil Engineers – Engineering History and Heritage*, 162(1), 13-18.

Faisal A, Majid TA, Hatzigeorgiou GD (2013). Investigation of story ductility demands of inelastic concrete frames subjected to repeated earthquakes. *Soil Dynamics and Earthquake Engineering*, 44, 42-53.

Fragiacomo M, Amadio C, Macorini L (2004). Seismic response of steel frames under repeated earthquake ground motions. *Engineering Structures*, 24, 2021-2035.

Ghallab A (2020). Simulation of cracking in high concrete gravity dam using the Extended Finite Elements by ABAQUS. *American Journal of Mechanics and Applications*, 8(1), 7-15.

Gopalaratnam VS, Shah SP (1985). Softening response of plain concrete in direct tension. *Journal of the American Concrete Institute*, 82(3), 310-323.

Guo X, Zhang Z, Chen ZQ (2020). Mainshock-integrated aftershock vulnerability assessment of bridge structures. *Applied Sciences*, 10, 6843.

Hacıefendioğlu K, Akköse M, Bayraktar A, Dumanoğlu AA (2015). Shear strain related non-linear stochastic dynamic analysis of rock-fill dams. *Challenge Journal of Structural Mechanics*, 1(2), 59-64.

Hariri-Ardebili MA, Kianoush MR (2014). Integrative seismic safety evaluation of a high concrete arch dam. *Soil Dynamics and Earthquake Engineering*, 67, 85-101.

Hariri-Ardebili MA, Saouma VE (2016). Collapse fragility curves for concrete dams: comprehensive study. *Journal of Structural Engineering*, 142(10), 04016075.

Hatzigeorgiou GD (2010). Behavior factors for nonlinear structures subjected to multiple near-fault earthquakes. *Computers & Structures*, 88, 309-321.

Hatzigeorgiou GD, Beskos DE (2009). Inelastic displacement ratios for SDOF structures subjected to repeated earthquakes. *Engineering Structures*, 31, 2744-2755.

Huang J (2014). Effects of near-fault ground motions on the seismic performance of concrete gravity dams. *Proceedings of the 9th International Conference of Structural Dynamics*, *EURODYN 2014*, Porto, Portugal.

International Commission on Large Dams (2023). World Register of Dams (Database Presentation), International Commission on Large Dams. https://www.icold-cigb.org/GB/world_register/database_presentation.asp [accessed 21-2-2024].

Khanal A (2019). Seismic Performance of Earth Slopes Subjected to Earthquake Mainshock – Aftershock Sequences. *M.Sc. thesis*, University of Texas at Tyler, Texas, USA.

Leger P, Leclerc M (1996). Evaluation of earthquake ground motions to predict cracking response of gravity dams. *Engineering Structures*, 18(3), 227-239.

Li Y, Song R, van de Lindt JW (2014). Collapse fragility of steel structures subjected to earthquake mainshock-aftershock sequences. *Journal of Structural Engineering*, 140(12), 04014095.

Lokke A, Chopra AK (2013). Response Spectrum Analysis of Concrete Gravity Dams Including Dam-Water-Foundation Interaction. PEER Report 2013/17, Pacific Earthquake Engineering Research Center, Headquarters at the University of California, Berkeley.

Maekawa K, Okamura H, Pimanmas A (2003). Non-Linear Mechanics of Reinforced Concrete. 1st ed. CRC Press, London, UK.

Mangalathu S, Shokrabadi M, Burton HV (2019). Aftershock Seismic Vulnerability and Time-Dependent Risk Assessment of Bridges. PEER Report 2019/04, Pacific Earthquake Engineering Research Center, Headquarters at the University of California, Berkeley.

Meguro K, Tagel-Din H (2000). Applied element method for structural analysis: theory and application for linear materials. *Structural Engineering/Earthquake Engineering*, 17(1), 21s–35s.

Mignan A (2014). The debate on the prognostic value of earthquake foreshocks: A meta-analysis. *Scientific Reports*, 4, 4099.

Mooney CZ, Duval RD (1993). Bootstrapping: A Nonparametric Approach to Statistical Inference. Sage University Paper Series on Quantitative Applications in the Social Sciences, 07-095. Newbury Park, CA, USA.

Pang R, Xu B, Zhang X, Zhou Y, Kong X (2019). Seismic performance investigation of high CFRDs subjected to mainshock-aftershock sequences. *Soil Dynamics and Earthquake Engineering*, 116, 82-85.

Pekau OA, Zhu X (2008). Effect of seismic uplift pressure on the behavior of concrete gravity dams with a penetrated crack. *Journal of Engineering Mechanics*, 134(11), 991-999.

Pirooz RM, Habashi S, Massumi A (2021). Required time gap between mainshock and aftershock for dynamic analysis of structures. *Bulletin of Earthquake Engineering*, 19, 2643-2670.

RILEM TC 104 (1991). Damage classification of concrete structures. The state of the art report of RILEM Technical Committee 04-DCC activity. *Materials and Structures*, 24(142), 253-259.

Risk Management Solutions (2008). Risk Management Solutions Reconnaissance Report: The 2008 Wenchuan Earthquake: Risk Management Lessons and Implications. Risk Management Solutions, Newark, CA, USA.

Sadeghi MH, Moradloo J (2022). Seismic analysis of damaged concrete gravity dams subjected to mainshock-aftershock sequences. *European Journal of Environmental and Civil Engineering*, 26, 2417-2438.

Sommerfeld A (1949). Partial Differential Equations in Physics. 1st ed. Academic Press, New York.

Soysal Albostan BF (2021). Discrete Element Based Analyses of Structure-Reservoir Problem for Gravity Dams. *Ph.D. thesis*, Middle East Technical University, Ankara, Turkey.

Soysal BF, Arici Y, Tuncay K (2023). A modified applied element model for the simulation of plain concrete behaviour. *Magazine of Concrete Research*, 75, 325-338.

Soysal BF, Arici Y (2024). The use of discrete element models for the seismic assessment of concrete gravity dams. *Structures*, 70, 107831.

SRC (n.d.). Dams & earthquakes. Seismology Research Centre. https://www.src.com.au/earthquakes/seismology-101/dams-earthquakes [accessed 21-2-2024].

Toikka L, Grover L, Hull A, Rossiter M (2019). Site-specific seismic analysis for concrete gravity dams: a case study from Ontario. *12th Canadian Conference on Earthquake Engineering*, Quebec, QC, Canada, 1-8.

United States Geological Survey (2015). Magnitude 7.8 earthquake Nepal Aftershocks. United States Geological Survey. https://www.usgs.gov/news/featured-story/magnitude-78-earthquake-nepal-aftershocks [accessed 21-2-2024].

Wang G, Wang Y, Lu W, Yan P, Zhou W, Chen M (2017). Damage demand assessment of mainshock-damaged concrete gravity dams subjected to aftershocks. *Soil Dynamics and Earthquake Engineering*, 98, 141-154.

Wang M, Chen J, Wu L, Song B (2018). Hydrodynamic pressure on gravity dams with different heights and the Westergaard correction formula. *International Journal of Geomechanics*, 18(10), 04018134.

Wang G, Wang Y, Lu W, Yan P, Chen M (2020). Earthquake direction effects on seismic performance of concrete gravity dams to mainshock-aftershock sequences. *Journal of Earthquake Engineering*, 24, 1134-1155.

Wang X, Bathe KJ (1997). Displacement/pressure based mixed finite element formulations for acoustic fluid-structure interaction problems. *International Journal for Numerical Methods in Engineering*, 40, 2001-2017.

Wei Q, Shen L, Dunai L, Kövesdi B, Elqudah S, Cao M (2024). Quantitative evaluation on the effects of the spatial variability in concrete materials on seismic damage of concrete gravity dams. *Engineering Fracture Mechanics*, 307, 110287.

Wen R, Zhou Z, Li X, Yang C, Wang Y, Liu Q, Cui J (2009). The strong ground motion observation for the Wenchuan aftershock. *Earthquake Science*, 22, 181–187.

Zhai Y, Zhang L, Bi Z, Zhang H, Cui, B (2022). Seismic performance evaluation of AAR-affected concrete gravity dams under main aftershock sequence. *Soil Dynamics and Earthquake Engineering,* 157, 107258.

Zhang L, Zhai Y, Chen D, Cui X (2019). Study on influence of dam foundation damage on seismic safety of gravity dam under combined action of main shock and aftershock. *IOP Conference Series: Earth and Environmental Science*, 304, 042063.

Zhang L, Zhai Y, Cui B, Tang Y, Bi Z (2021). A novel method for constructing main-aftershock sequences and its application in the global damage accumulation effects analysis of gravity dams. *Shock and Vibration*, 3, 1-12.

Zhang S, Wang G, Sa W (2013). Damage evaluation of concrete gravity dams under mainshock-aftershock seismic sequences. *Soil Dynamics and Earthquake Engineering*, 50, 16-27.